Supplementary Information (SI) for Journal of Materials Chemistry C.
This journal is © The Royal Society of Chemistry 2025

Supporting Information

Benzo-Extended N^N^N-Chelated Tetracoordinate Boron Hetero[8]Helicene Featuring an Inner N–B–N Helical Rim for Circularly Polarized TADF

Yili He,[#] Haoting Yang,[#] Yuanchun Yue,[#] Xiangqing Gan, Shuai Xiao, Xian Chen, Shaobiao Zhu, Danrui Wan, Renze He, Han Si,[*] Guoyun Meng,[*] Pangkuan Chen and Junqiao Ding[*]

Y. He, H. Yang, Y. Yue, X. Gan, S. Xiao, X. Chen, S. Zhu, D. Wan, R. He, Dr. H. Si, Dr. G. Meng, Prof. J. Ding

School of Chemical Science and Technology, Yunnan University, Kunming 650091, P. R. China

E-mail: sihan94720@outlook.com; mengguoyun@ynu.edu.cn; dingjunqiao@ynu.edu.cn

Y. Yue, D. Wan, Prof. J. Ding

Southwest United Graduate School, Kunming 650092, P. R. China

Prof. P. Chen

Beijing Key Laboratory of Photoelectronic/Electrophotonic Conversion Materials, Key Laboratory of Medical Molecule Science and Pharmaceutical Engineering of the Ministry of Industry and Information Technology, School of Chemistry and Chemical Engineering, Beijing Institute of Technology, Beijing 102488, P. R. China

[#]These authors contributed equally to this work.

Table of Contents

1. Experimental Section

1.1 General Information. All reagents used for reaction, purification, and measurements were purchased from Shanghai Bide Medical Technology Co., Ltd. All other reagents used for device fabrication were purchased from Jilin Optical and Electronic Materials Co., Ltd. These materials were received and used without further purification. The other reagents and solvents were used as received from commercial sources without further purification. ^{1}H NMR spectra were measured by a Bruker Avance 400 MHz at room temperature in deuterated dichloromethane and chloroform, respectively, with tetramethylsilane as the internal standard. MALDI-TOF-MS data was performed on a Bruker rapifleX MALDI-TOF instrument in positive detection modes. The thermogravimetric analysis (TGA) was performed on a METTLER-TOLEDO TGA/DSC1/1600 thermal analyzer at a heating rate of 10 °C min^{-1} in nitrogen. Chiral high-performance liquid chromatography (HPLC) was implemented on a SHIMADZU LC-30ADsf, column: Chiralpak IG-3, 50 × 4.6 mm, I.D., particle size 3 um. Method: IG-3-EtOH (DEA)-20-60-3ML-35T.

1.2 Computational methods. The calculations were performed with the Gaussian 09 package, using the density functional theory (DFT) and time-dependent density functional theory (TD-DFT) method with the B3LYP functional.[1-3] The structures were optimized using DFT (S_0 state) methods with a 6-31G(d) basis set. Natural transition orbital analyses[4] were also performed to examine the nature of the excited states. Electron-hole analysis was carried out using the Multiwfn software.[5] On the basis of predicting the transition state in advance, the transition state structure is optimized with the TS keyword, the first-order saddle point is found, and the single point energy is calculated at PBE0/6-311G(d,p) level, and the Gibbs free energy is further calculated.

1.3 Measurement of absorption and emission characteristics. The concentration of the solution (1×10^{-5} M) was prepared by stepwise dilution for solution state measurements. Thin films for photophysical characterization were prepared by thermal evaporation on quartz substrates at 1-2 Å sec^{-1} in a vacuum chamber with a base pressure of < 10^{-5} torr. UV-vis absorption and PL spectra were measured using UV-2600 (Shimadzu) and FluoroMax-4P

(Horiba) instruments at 77 and 298 K. The PLQYs were obtained with an absolute photoluminescence quantum yield measurement system Hamamatsu C9920-03G in an integrating sphere. The solution sample was bubbled with nitrogen for 10 minutes before measurement, while the films were measured in air. The transient spectra were collected on an Edinburgh Fluorescence Spectroscopy FLS1000.

1.4 Electrochemical measurements. Cyclic voltammetry was performed on a CHI 660 instrument, using a platinum (Pt) electrode as the working electrode, a Pt wire as the auxiliary electrode and an Ag/Ag^+ electrode as the reference electrode. The oxidation/reduction potentials were measured in dry dichloromethane/DMF solutions with 0.1 M of $TBAPF_6$ (tetrabutylammonium hexafluorophosphate) as a supporting electrolyte at a scan rate of 100 mV s^{-1}.

$E_{HOMO} = -(E_{[onset,ox\ vs.\ Fc^+/Fc]} + 4.8)$ (eV) $E_{LUMO} = -(E_{[onset,red\ vs.\ Fc^+/Fc]} + 4.8)$ (eV)

1.5 The calculation of rate constants. The prompt fluorescence and delayed fluorescence quantum yield ratio (Φ_{PF} and Φ_{DF}) were determined from the total PL quantum efficiency (Φ_{PL}) and the proportion of the integrated area of each component in the transient spectra to the total integrated area, r_{PF} and r_{DF} are individual component ratios for prompt and delayed fluorescence. The quantum efficiencies and rate constants were determined using the following equations according to Adachi's method.[6]

(1) $\Phi_{PF} = \Phi_{PL} r_{PF}$ $r_{PF} = \tau_1 A_1/(\tau_1 A_1 + \tau_2 A_2)$

(2) $\Phi_{DF} = \Phi_{PL} r_{DF}$ $r_{DF} = \tau_2 A_2/(\tau_1 A_1 + \tau_2 A_2)$

(3) $k_r = \Phi_{PF}/\tau_{PF}$

(4) $k_{ISC} = (1-\Phi_{PF})/\tau_{PF}$

(5) $k_{RISC} = \Phi_{DF}/(k_{ISC}.\tau_{PF}.\tau_{DF}.\Phi_{PF})$

1.6 OLED fabrication and measurement characteristics. All compounds were subjected to temperature-gradient sublimation under a high vacuum before use. OLEDs were fabricated on the ITO-coated glass substrates with multiple organic layers sandwiched between the transparent bottom indium-tin-oxide (ITO) anode and the top metal cathode. Before device

fabrication, the ITO glass substrates were pre-cleaned carefully. All material layers were deposited by vacuum evaporation in a vacuum chamber with a base pressure of 10^{-6} torr. The deposition system permits the fabrication of the complete device structure in a single vacuum pump-down without breaking the vacuum. The deposition rate of organic layers was kept at 0.1~0.2 nm s^{-1}. The doping was conducted by co-evaporation from separate evaporation sources with different evaporation rates. The current density, voltage, luminance, external quantum efficiency, electroluminescent spectra, and other characteristics were measured with a Keithley 2400 source meter and an absolute EQE measurement system in an integrating sphere at the same time. The EQE measurement system is Hamamatsu C9920-12, which is equipped with Hamamatsu PMA-12 Photonic multichannel analyzer C10027-02, whose longest detection wavelength is 1100 nm. The Lambertian distribution was measured under a constant voltage of 4.5 V using a light distribution measurement system (Hamamatsu C9920-11).

1.7 Synthesis

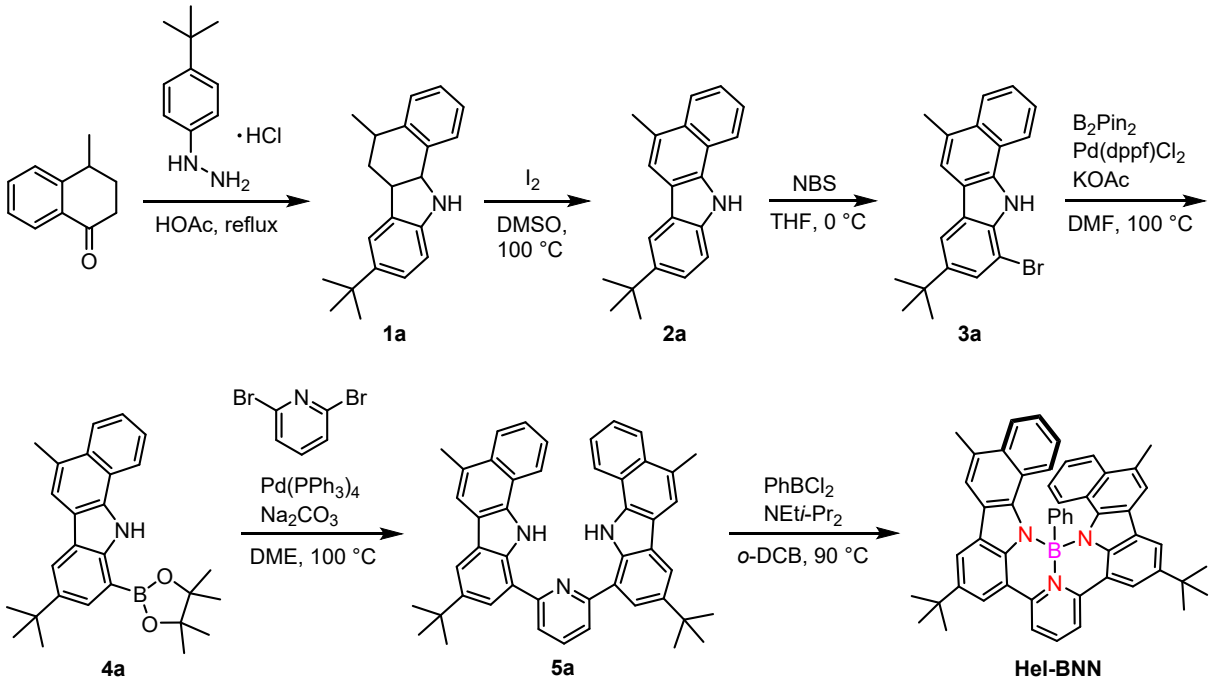

Scheme S1. The synthetic route of **Hel-BNN**.

Synthesis of 8-(tert-butyl)-5-methyl-6,6a,11,11a-tetrahydro-5H-benzo[a]carbazole (**1a**).

In a 500 mL three-necked flask, 4-tert-butylphenylhydrazine hydrochloride (31.3 g, 0.16

mol) and 1-methyl-4-methylene-1,2,3,4-tetrahydronaphthalene (25.0 g, 0.16 mol) were added in 250 mL of acetic acid under nitrogen. The mixture was heated to 100 °C and stirred for 8 h. Then, the mixture was poured into water, yielding a white precipitate. The solid was collected by filtration and extracted with CH_2Cl_2 three times. The organic phase was dried over $MgSO_4$, and the solvent was evaporated in vacuo. The crude product was purified by flash chromatography on silica gel, giving **1a** as a white solid, 33.54 g, yield of 71.9%. ^{1}H NMR (400 MHz, DMSO-d_6) δ (ppm): 11.26 (s, 1H), 7.63 (d, *J* = 7.4 Hz, 1H), 7.44 (s, 1H), 7.32–7.25 (m, 3H), 7.18 (d, *J* = 8.0, 2H), 3.38 (s, 1H), 3.20–2.97 (m, 2H), 2.75–2.69 (m, 1H), 1.35 (s, 9H), 1.25 (d, *J* = 6.9 Hz, 3H).

Synthesis of 8-(tert-butyl)-5-methyl-11H-benzo[a]carbazole (**2a**).

To a 500 mL three-necked flask equipped with compound **1a** (33.54 g, 0.12 mol) and iodine (7.3 g, 28.8 mmol), 250 mL of DMSO was added under nitrogen. The mixture was heated to 100 °C and stirred for 16 h. The reactant was poured into the sodium thiosulfate aqueous solution and extracted with CH_2Cl_2 three times. The solvent was evaporated in vacuo. The crude product was purified by flash chromatography on silica gel with petroleum ether/CH_2Cl_2 (5:1, v/v), and the product was purified by recrystallization to get **2a** as a white solid, 22.59 g, yield of 65.5%. ^{1}H NMR (400 MHz, $CDCl_3$) δ (ppm): 8.61 (s, 1H), 8.14 (dt, *J* = 7.5, 2.0 Hz, 2H), 8.10 (s, 1H), 8.01 (s, 1H), 7.63–7.56 (m, 2H), 7.51 (s, 2H), 2.82 (s, 3H), 1.48 (s, 9H).

Synthesis of 10-bromo-8-(tert-butyl)-5-methyl-11H-benzo[a]carbazole (**3a)**.

At room temperature, NBS (12.39 g, 69.59 mmol) was dissolved in THF (250 mL). The resulting solution was added dropwise to a 500 mL three-necked flask containing compound **2a** (20 g, 69.59 mmol) under an ice-water bath. Then, removed the ice and wrapped it with aluminum foil. The mixture was stirred for 16 h under nitrogen. Removing a portion of THF under reduced pressure. The residue was extracted with CH_2Cl_2 and water. The crude product was purified by flash chromatography on silica gel with petroleum ether / CH_2Cl_2 (5:1, v/v), and the product was purified by recrystallization to get **3a** as a white solid, 20.12 g, yield of 78.9%. ^{1}H NMR (400 MHz,$CDCl_3$) δ (ppm): 8.70 (s, 1H), 8.22 (d, *J* = 7.8 Hz, 1H), 8.14 (d, *J* = 8.1 Hz, 1H), 8.03 (d, *J* = 1.5 Hz, 1H), 7.96 (s, 1H), 7.66–7.59 (m, 3H), 2.81 (s, 3H), 1.46 (s,

9H).

Synthesis of 8-(tert-butyl)-10-(((3-methoxy-2,3-dimethylbutan-2-yl)oxy)boraneyl)-5-methyl-11H-benzo[a]carbazole (**4a)**

At room temperature, compound **3a** (15.45 g, 42.18 mmol), bis(pinacolato)diboron (B_2Pin_2, 12.85 g, 50.60 mmol), Pd(dppf)Cl_2 (1.54 g, 2.10 mmol), and KOAc (8.28 g, 84.36 mmol) were added to a 500 mL three-necked flask. The system was evacuated and purged with nitrogen three times. Then, 250 mL of DMF, previously degassed by bubbling nitrogen for 30 min, was added to the flask via syringe under nitrogen. The mixture was heated to 100 °C and stirred for 18 h. The reactant was extracted with CH_2Cl_2 three times. The crude product was purified by flash chromatography on silica gel with petroleum ether / CH_2Cl_2 (10:1, v/v), and the product was purified by recrystallization to get **4a** as a white solid, 12.34 g, yield of 70.7%. ^{1}H NMR (400 MHz, $CDCl_3$) δ (ppm): 9.75 (s, 1H), 8.24 (d, *J* = 1.8 Hz, 1H), 8.21 (d, *J* = 8.2 Hz, 1H), 8.14 (d, *J* = 8.2 Hz, 1H), 8.03 (s, 1H), 7.93 (d, *J* = 1.9 Hz, 1H), 7.66–7.62 (m, 1H), 7.59 (td, *J* = 7.6, 1.1 Hz, 1H), 2.83 (s, 3H), 1.49 (d, *J* = 5.0 Hz, 21H).

Synthesis of 2,6-bis(8-(tert-butyl)-5-methyl-11H-benzo[a]carbazol-10-yl)pyridine (**5a**)

At room temperature, compound **4a** (0.87 g, 2.11 mmol), along with K_2CO_3 (0.73 g, 5.28 mmol), Pd(PPh_3)$_4$ (24.27 mg, 21.00 μmol), and 2,6-dibromopyridine (250.00 mg, 1.06 mmol), was placed in a 100 mL three-necked flask. The system was evacuated and purged with nitrogen three times. Then, 50 mL of DME and 10 mL water, previously degassed by bubbling nitrogen for 30 min, was added to the flask via syringe under nitrogen. The mixture was heated to 100 °C and stirred for 3 h. After cooling to room temperature, the reaction mixture was poured into water. After filtration, extracted with CH_2Cl_2 three times. The crude product was purified by flash chromatography on silica gel with petroleum ether/CH_2Cl_2 (10:1, v/v), and the product was purified by recrystallization to get **5a** as a white solid, 1.11 g, yield of 80.9%. ^{1}H NMR (400 MHz, CD_2Cl_2) δ: 11.24 (s, 2H), 8.35 (s, 2H), 8.15 (d, *J* = 6.1 Hz, 5H), 8.08 (s, 2H), 7.77 (d, *J* = 8.4 Hz, 2H), 7.03 (t, *J* = 7.0 Hz, 2H), 6.95 (d, *J* = 8.2 Hz, 2H), 6.40 (t, *J* = 7.2 Hz, 2H), 2.75 (s, 6H), 1.62 (s, 18H). ^{13}C NMR (101 MHz, CD_2Cl_2) δ: 142.84, 138.22, 134.99, 134.84, 131.32, 125.90, 125.58, 124.42, 124.35, 124.00, 121.39, 121.31, 121.09, 120.58, 118.87,

117.63, 117.39, 34.90, 31.91, 19.62.

Synthesis of **Hel-BNN**

At room temperature, compound **5a** (1.0 g, 1.538 mmol) was added to a 100 mL high-pressure reaction tube, followed by $PhBCl_2$ (0.22 mL, 0.26 g, 1.64 mmol) and $NEt(i\text{-}Pr)_2$ (0.50 mL, 0.398 g, 3.06 mmol). The system was evacuated and purged with nitrogen three times. An *o*-DCB solution (20 mL) was degassed with nitrogen for 30 min and then injected into the tube. The mixture was heated to 90 °C, and a blast shield was installed outside the reactor. The reaction was stirred under nitrogen protection for 24 h. After removing the solvent in vacuo, the crude product was purified by flash chromatography on silica gel with petroleum ether/CH_2Cl_2 (10:1, v/v), and the product was purified by recrystallization to get **Hel-BNN** as an orange solid, 0.69 g, yield of 61%. ^{1}H NMR (400 MHz, CD_2Cl_2) δ (ppm): 8.47 (s, 1H), 8.43 (s, 1H), 8.26 (s, 1H), 8.06 (d, *J* = 7.9 Hz, 2H), 7.99 (s, 1H), 7.95 (d, *J* = 7.8 Hz, 1H), 7.90 (s, 1H), 7.42 (d, *J* = 8.2 Hz, 1H), 7.35 (s, 1H), 6.73 (t, *J* = 7.6 Hz, 1H), 6.65 (t, *J* = 7.6 Hz, 1H), 6.55 (s, 1H), 6.46 (t, *J* = 7.5 Hz, 2H), 6.00–5.91 (m, 2H), 2.56 (s, 6H), 1.60 (s, 9H), 1.54 (s, 9H). ^{13}C NMR (101 MHz, CD_2Cl_2) δ (ppm): 151.98, 148.56, 145.69, 144.64, 143.95, 142.46, 140.56, 136.53, 131.82, 131.59, 126.78, 126.68, 126.51, 125.74, 125.71, 125.45, 124.93, 124.85, 123.64, 123.44, 123.40, 123.18, 122.78, 122.10, 121.26, 120.45, 120.26, 120.14, 119.97, 118.89, 118.84, 118.37, 118.09, 117.77, 113.12, 35.19, 35.04, 32.02, 31.95, 29.69, 19.78, 19.46. MALDI-TOF: Calculated: 735.3785, Found: 735.3866.

2. Supplementary figures and tables

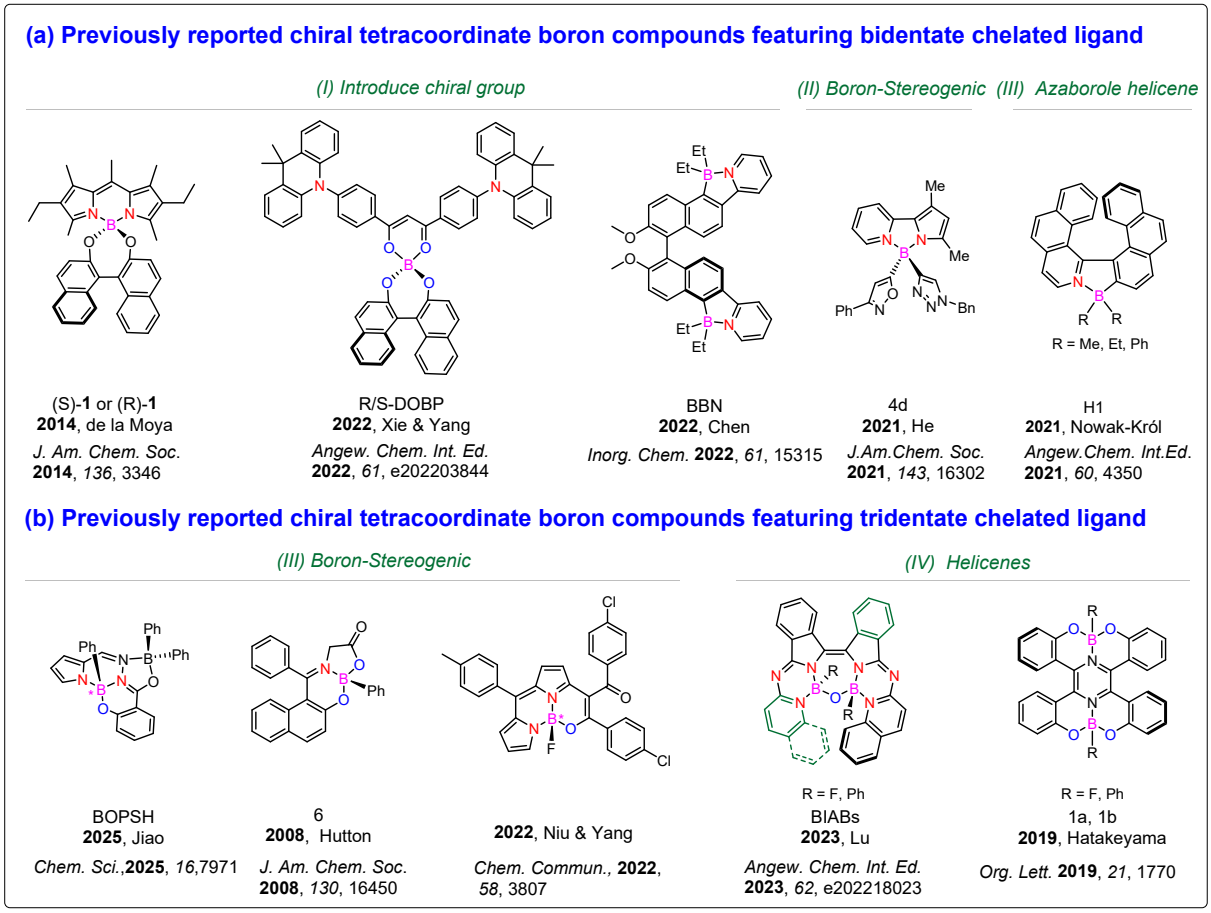

Scheme S2. Representative chiral tetracoordinate boron compounds.

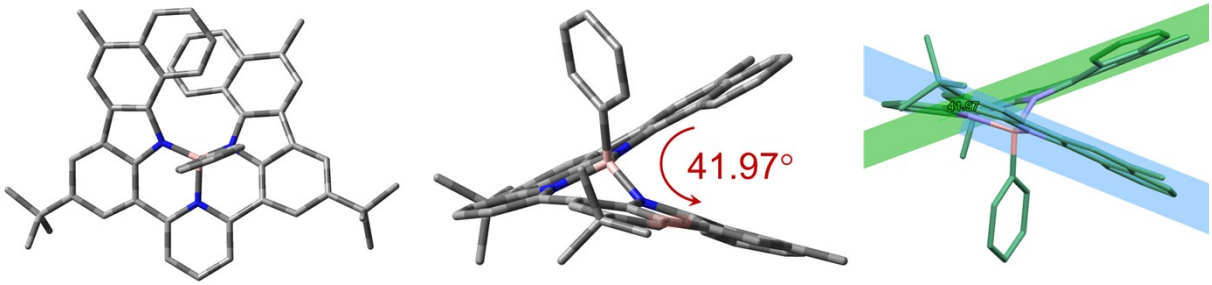

Figure S1. Optimized ground-state molecular conformation and dihedral angle of the helical configuration.

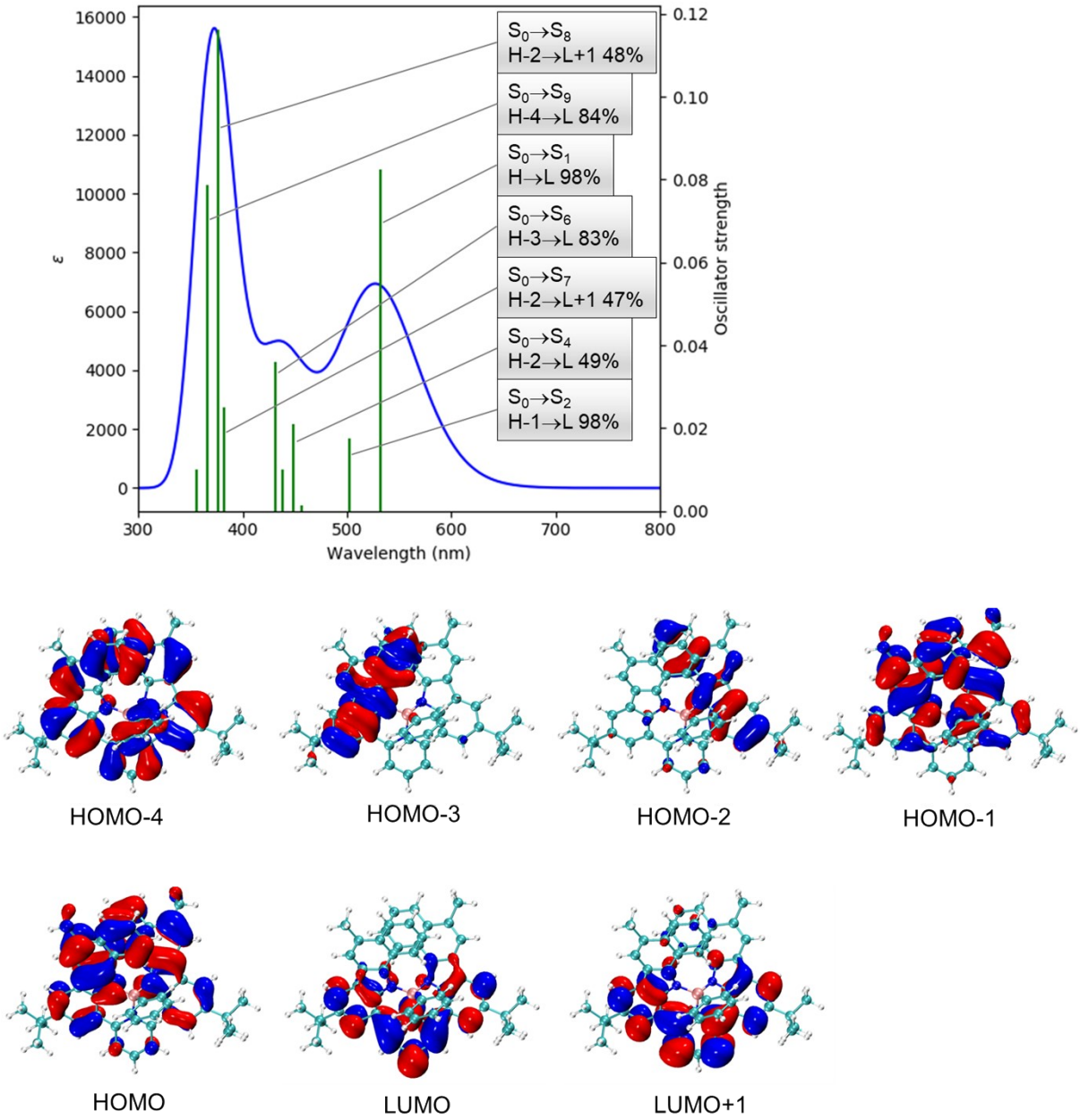

Figure S2. Simulated absorption spectra for **Hel-BNN** from first 10 singlet excited states calculated at B3LYP 6-31G(d) level and the corresponding frontier orbital distributions.

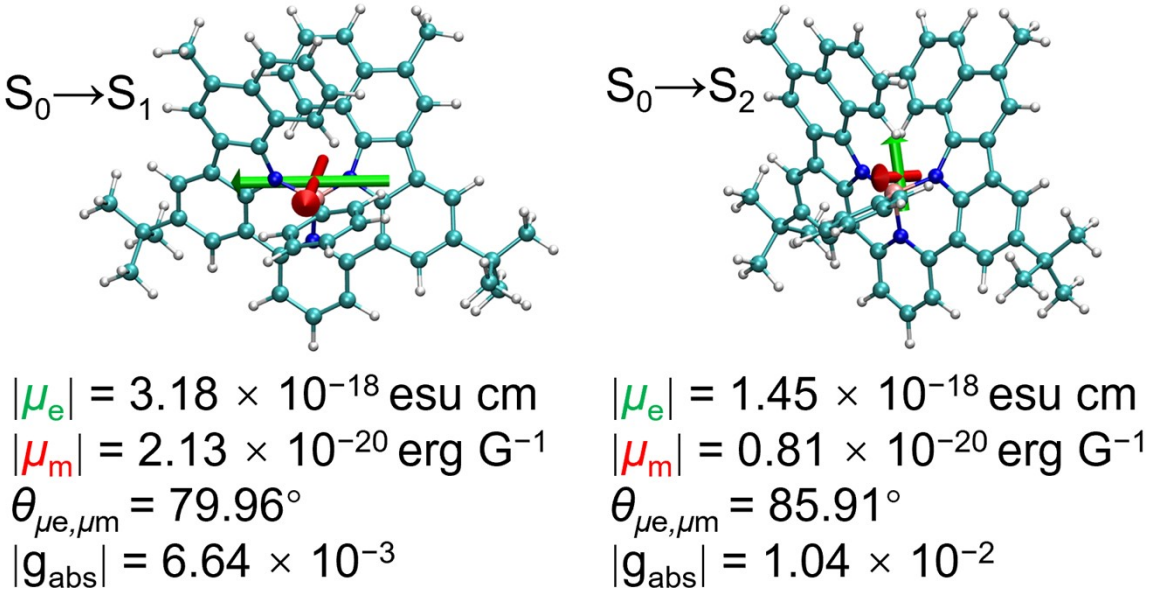

Figure S3. TD-DFT-calculated results of *M*-**Hel-BNN** with the electric (μ) and magnetic (m) transition dipole moments. For clarity, the length of the m vector is amplified 3 and 3 times for the $S_0 \rightarrow S_1$ and $S_0 \rightarrow S_2$ transitions, respectively.

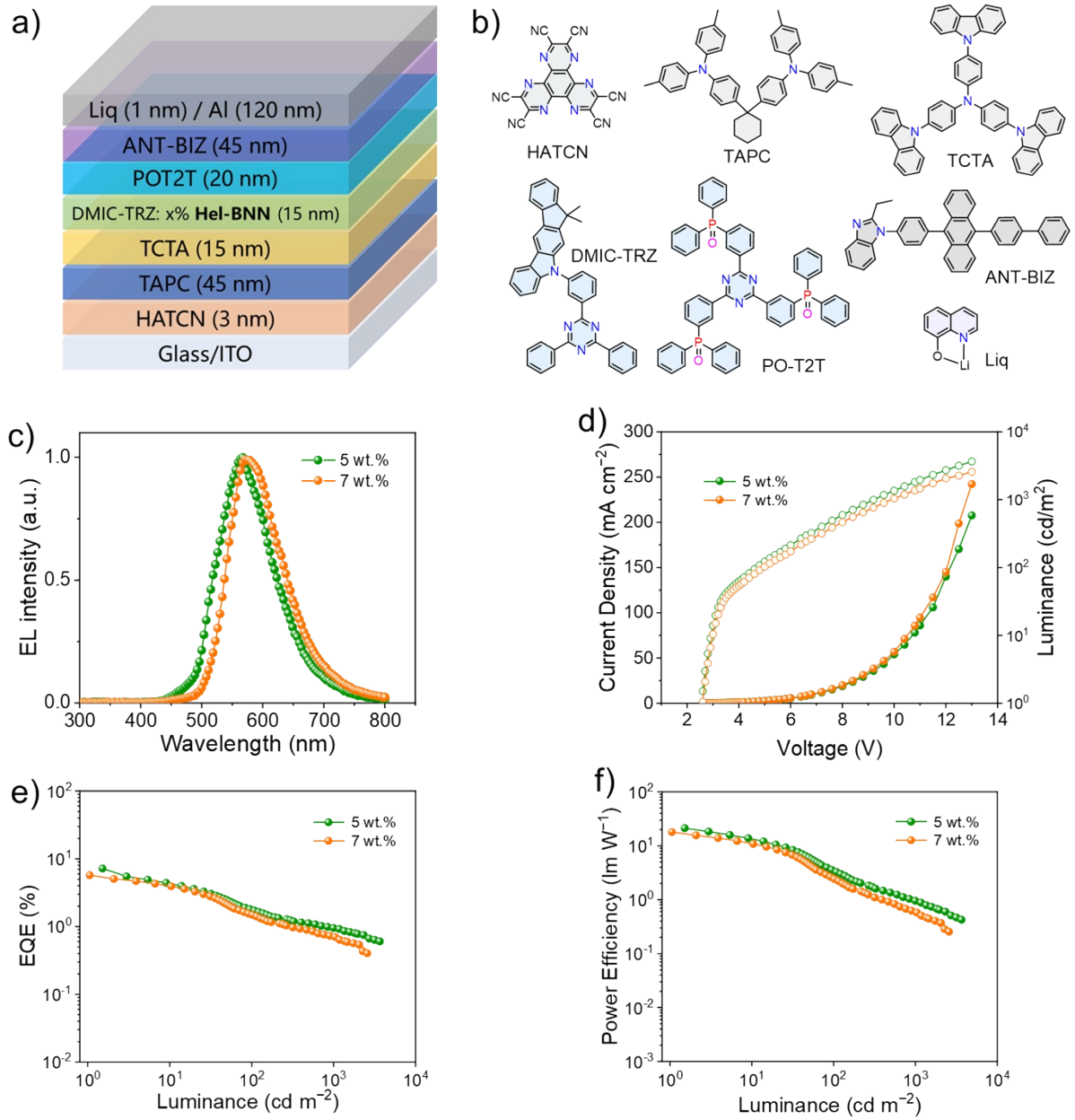

Figure S4. (a) OLED device structure. (b) The structures of the functional layers in the device. (c) EL spectrum under 1000 cd cm^{-2}. (d) Luminance-voltage-current density characteristics for the device. (e) EQE versus luminance curves of the device. (f) PE versus luminance curves of the device.

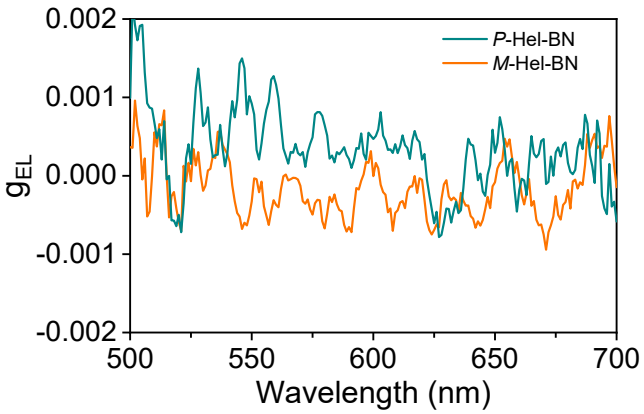

Figure S5. g_{EL} factors of CP-OLEDs based on *M*-and *P*-**Hel-BNN**.

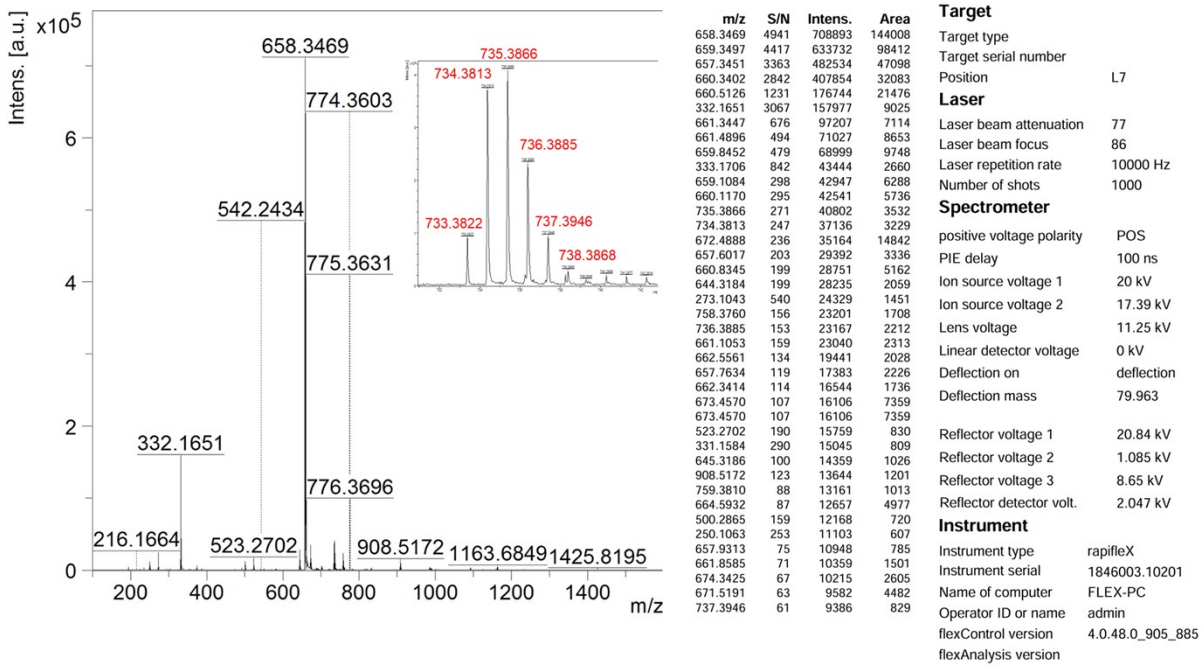

m/z	S/N	Intens.	Area
658.3469	4941	708893	144008
659.3497	4417	633732	98412
657.3451	3363	482534	47098
660.3402	2842	407854	32083
660.5126	1231	176744	21476
332.1651	3067	157977	9025
661.3447	676	97207	7114
661.4896	494	71027	8653
659.8452	479	68999	9748
333.1706	842	43444	2660
659.1084	298	42947	6288
660.1170	295	42541	5736
735.3866	271	40802	3532
734.3813	247	37136	3229
672.4888	236	35164	14842
657.6017	203	29392	3336
660.8345	199	28751	5162
644.3184	199	28235	2059
273.1043	540	24329	1451
758.3760	156	23201	1708
736.3885	153	23167	2212
661.1053	159	23040	2313
662.5561	134	19441	2028
657.7634	119	17383	2226
662.3414	114	16544	1736
673.4570	107	16106	7359
673.4570	107	16106	7359
523.2702	190	15759	830
331.1584	290	15045	809
645.3186	100	14359	1026
908.5172	123	13644	1201
759.3810	88	13161	1013
664.5932	87	12657	4977
500.2865	159	12168	720
250.1063	253	11103	607
657.9313	75	10948	785
661.8585	71	10359	1501
674.3425	67	10215	2605
671.5191	63	9582	4482
737.3946	61	9386	829

Figure S6. Mass spectrometry of **Hel-BNN**. The molecular ion peak at 658.3469 corresponds to a derivative of the **Hel-BNN** in which the phenyl group attached to the boron center has been lost.

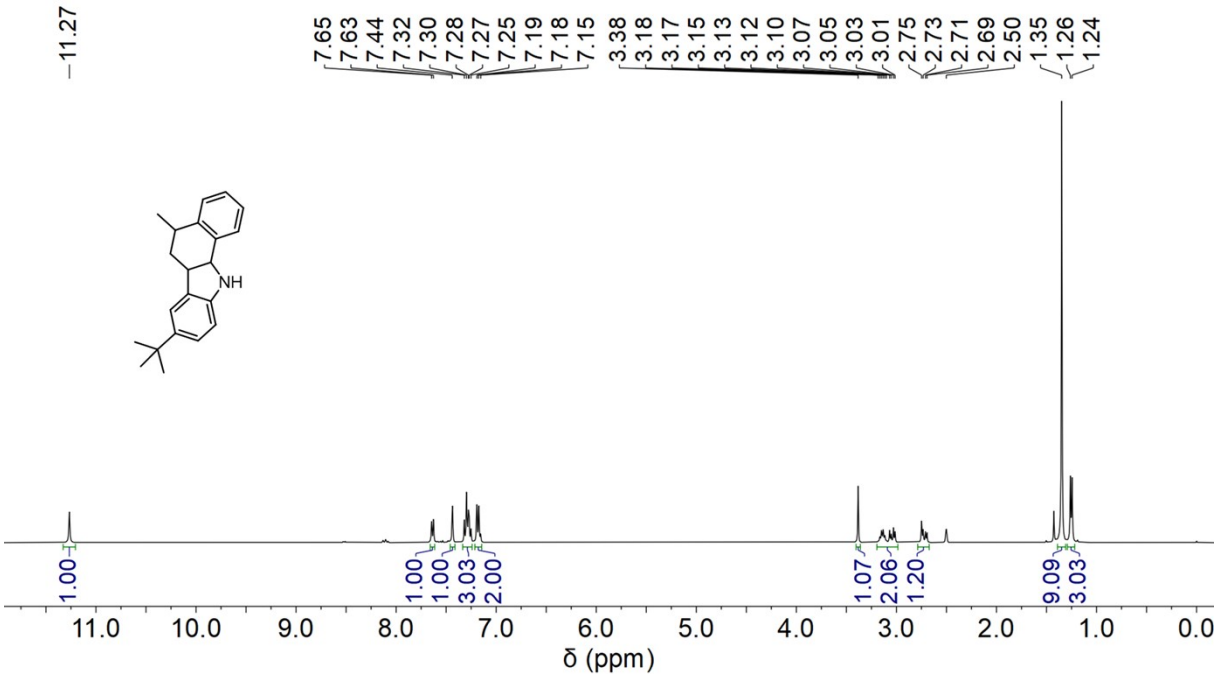

Figure S7. ^{1}H NMR spectrum of **1a** in DMSO-d_6.

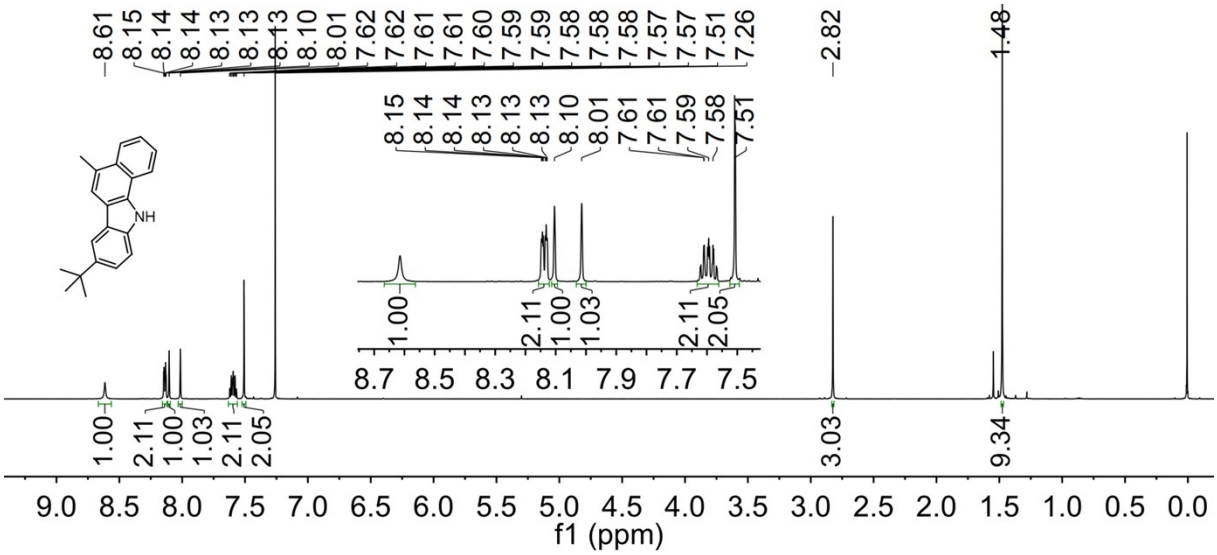

Figure S8. ^{1}H NMR spectrum of **2a** in $CDCl_3$.

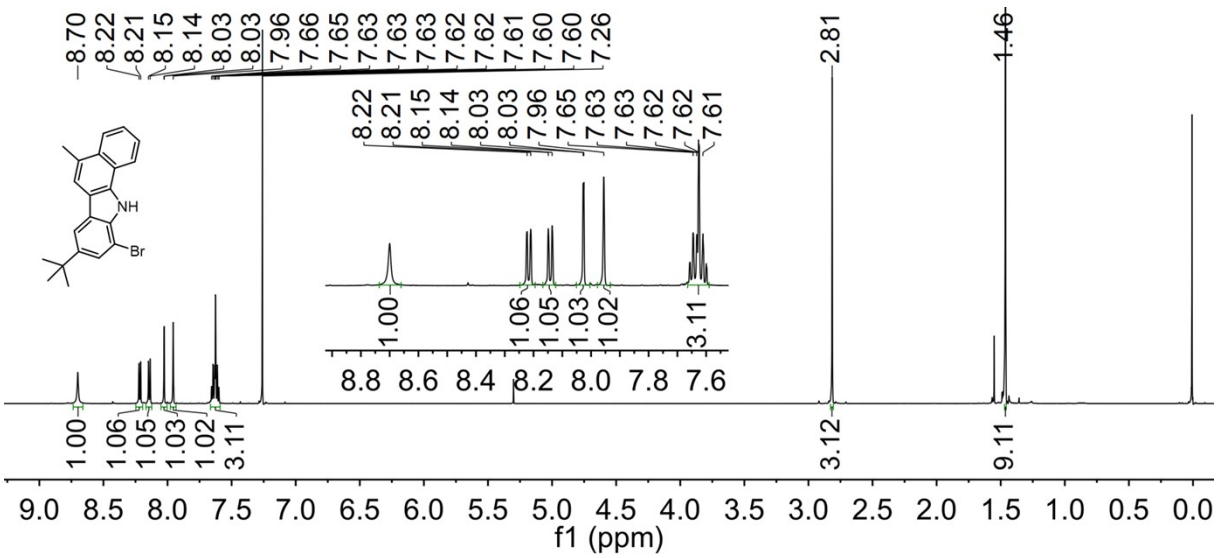

Figure S9. ^{1}H NMR spectrum of **3a** in $CDCl_3$.

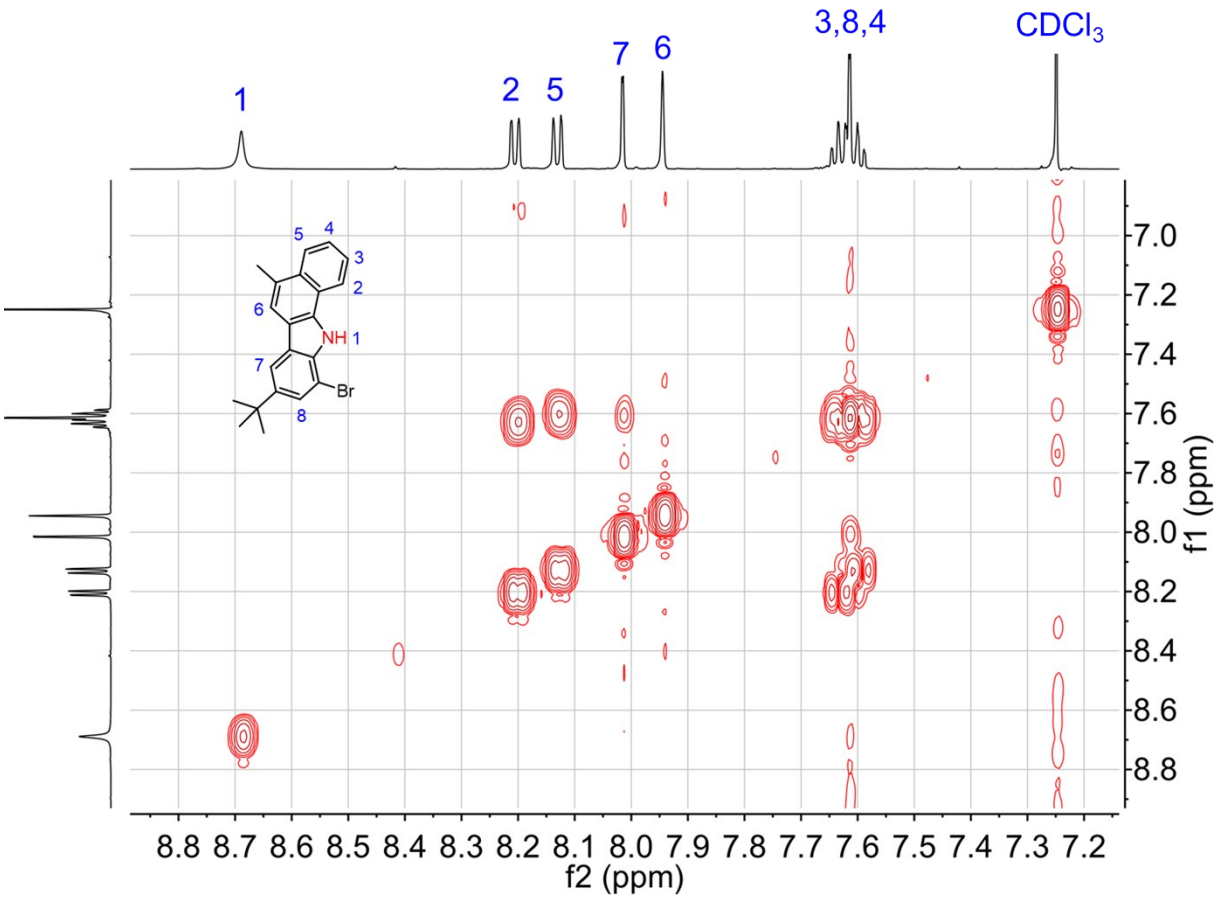

Figure S10. ^{1}H-^{1}H COSY NMR spectrum of **Hel-BNN** in $CDCl_3$.

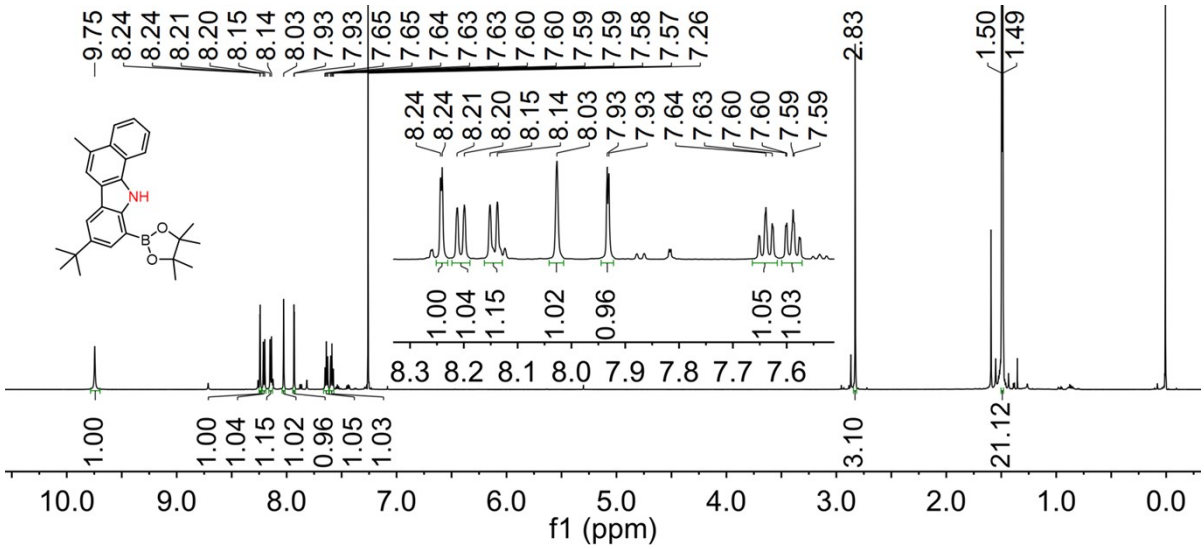

Figure S11. ^{1}H NMR spectrum of **4a** in $CDCl_3$.

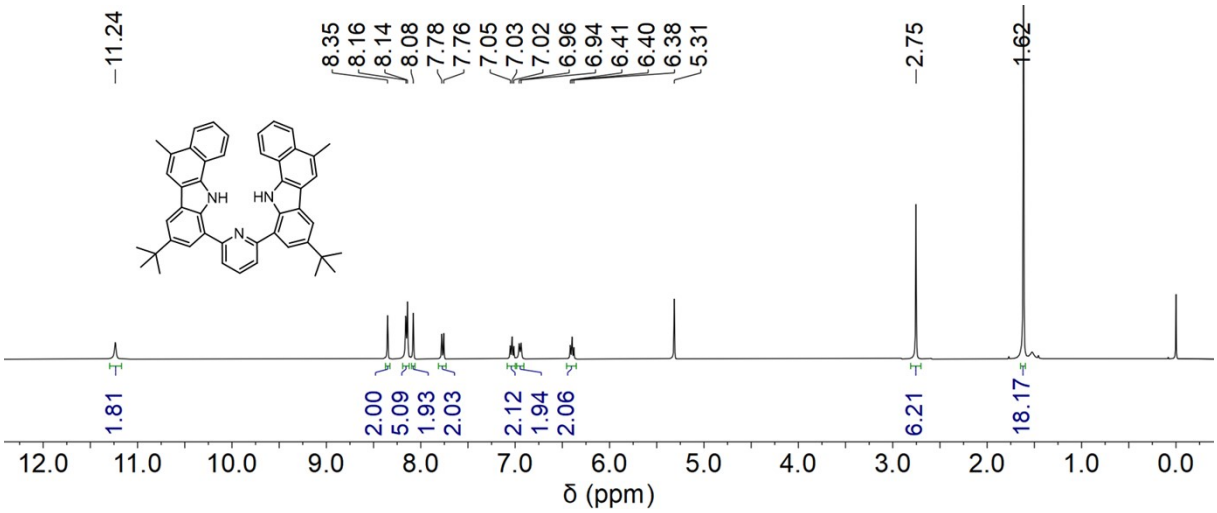

Figure S12. ^{1}H NMR spectrum of **5a** in CD_2Cl_2.

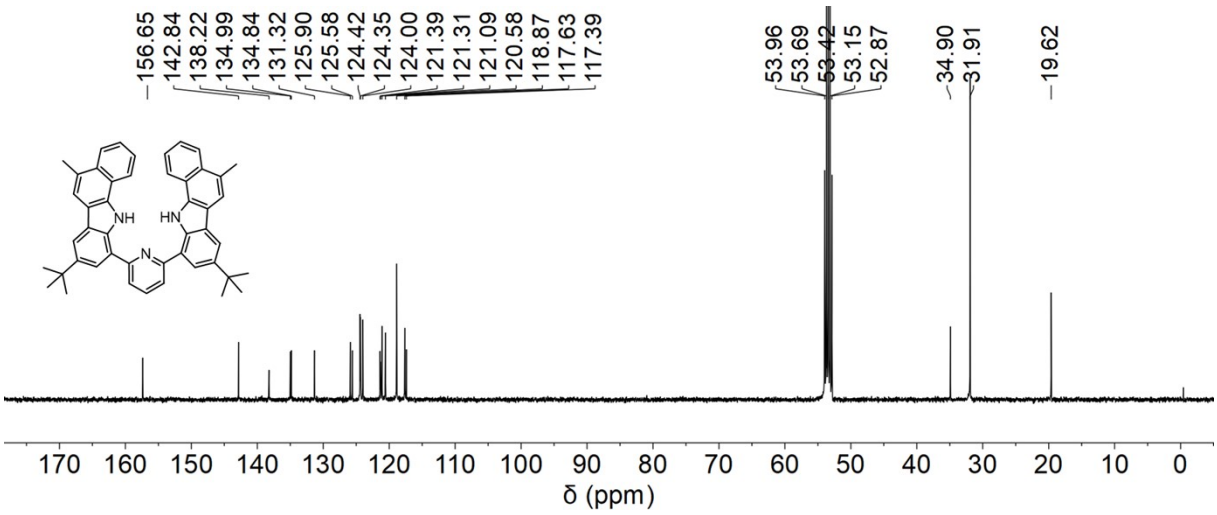

Figure S13. ^{13}C NMR spectrum of **5a** in CD_2Cl_2.

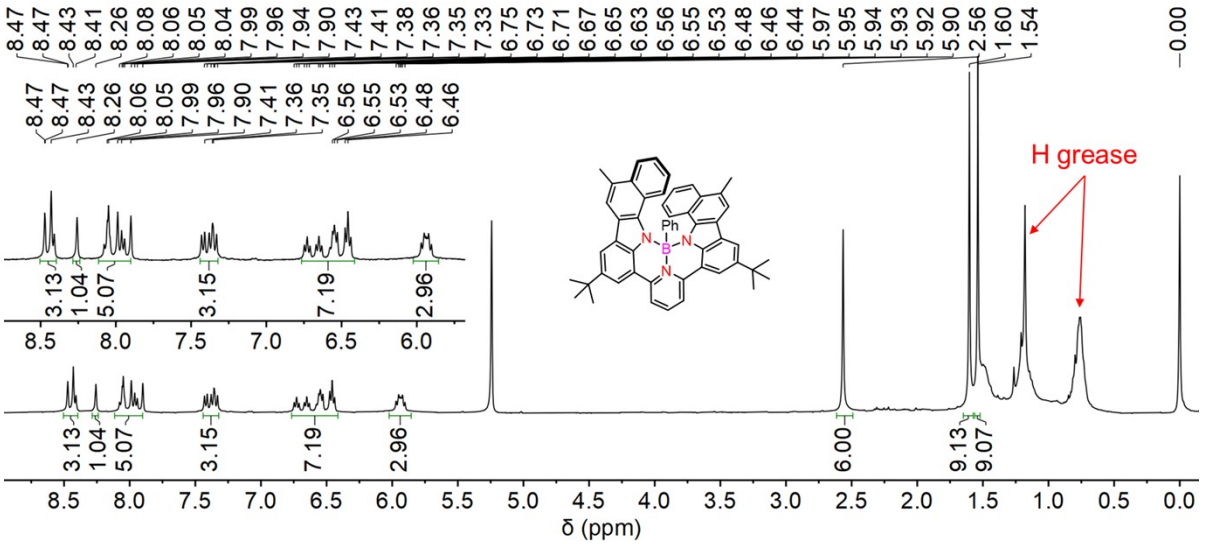

Figure S14. ^{1}H NMR spectrum of **Hel-BNN** in CD_2Cl_2.

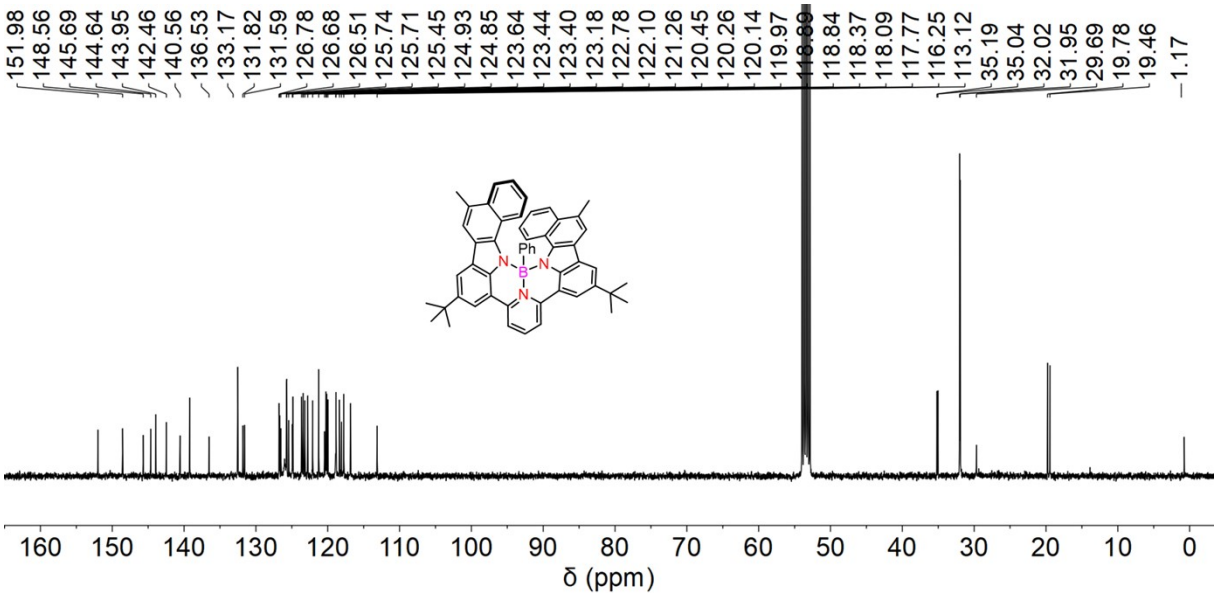

Figure S15. ^{13}C NMR spectrum of **Hel-BNN** in CD_2Cl_2.

Table S1 TD-DFT calculated electronic transitions for **Hel-BNN** along with their corresponding excitation energies and oscillator strengths.

Spin State	Transition Configuration	Excitation Energy (nm, eV)	Oscillator Strength
S_1	HOMO → LUMO (98%)	532.64 (2.33)	0.0823
S_2	HOMO-1 → LUMO (98%)	502.58 (2.48)	0.0175
S_3	HOMO → LUMO+1 (97%)	456.70 (2.71)	0.0013
S_4	HOMO-2 → LUMO (49%)	448.58(2.76)	0.0209

	HOMO-1 → LUMO+1 (37%)		
S_5	HOMO-2 → LUMO (36%) HOMO-1 → LUMO+1 (60%)	438.65 (2.83)	0.0099
S_6	HOMO-3 → LUMO (83%)	430.79 (2.88)	0.0361
S_7	HOMO-3 → LUMO+1 (47%) HOMO-2 → LUMO+1 (47%)	381.90 (3.25)	0.0249
S_8	HOMO-3 → LUMO+1 (47%) HOMO-2 → LUMO+1 (48%)	376.31 (3.29)	0.1163
S_9	HOMO-4 → LUMO (84%)	365.89 (3.39)	0.0787
S_{10}	HOMO-5→ LUMO (91%)	355.96 (3.48)	0.0100

Table S2. Summary of the device performances of the OLEDs based on **Hel-BNN**.

Device	λ_{EL} [a] [nm]	V_{on} [b] [V]	L_{max} [c] [cd m^{-2}]	CE [d] [cd A^{-1}]	PE [e] [lm W^{-1}]	EQE [f] [%]	CIE (x,y) [a]
5 wt.% Hel-BNN	567	2.6	3658	17.57/5.25/–	21.23/3.58/–	7.19/1.81/–	(0.437, 0.520)
7 wt.% Hel-BNN	572	2.6	2571	14.91/3.86/–	18.02/2.42/–	5.72/1.48/–	(0.493, 0.490)
20 wt.% PO-01 :2 wt.% Hel-BNN	567	2.5	68300	59.44/55.77/50.17	74.69/48.67/34.26	21.92/17.78/15.96	(0.501, 0.490)

[a] Value taken at a L = ca.1000 cd m^{-2}; [b] V_{on}: turn-on voltage; [c] Max. luminescence; [d] Current efficiency (CE): maximum, and values at 100 and 1000 cd m^{-2}; [e] Power efficiency (PE): maximum, and values at 100 and 1000 cd m^{-2}; [f] External quantum efficiency (EQE): maximum, values at 100 and 1000 cd m^{-2}.

Table S3. Summary of the representative CPL-active B,N-based emitters reported in literature.

Emitters	λ_{PL} [a] [nm]	$FWHM_{PL}$ [nm]	PLQY [%]	$\lvert g_{PL}\rvert$ [$\times10^{-3}$]	λ_{EL} [nm]	$FWHM_{EL}$ [nm]	EQE_{max} [%]	$\lvert g_{EL}\rvert$ [$\times10^{-3}$]	Refs.
DB-O	443	24	91	1.4	445	24	27.5	0.22	[7]
DB-S	444	23	95	1.5	447	24	29.3	0.26	[7]
(R/S)-DOBN	453	21	91	1.0	459	38	23.9	0.9	[8]
(R/S)-DOBNT	459	21	96	0.9	464	35	25.6	1.0	[8]
(R/S)-Czp-tBuCzB	478	23	98	1.6	479	24	32.1	1.54	[9]
(R/S)-OBN-2CN-BN	493	22	99	0.9	496	30	29.4	1.3	[10]

(R/S)-BN-MeIAc	497	30	96	0.32	504	33	37.2	0.27	[11]
(R/S)-Czp-POAB	498	36	93	1.4	513	48	28.7	1.30	[9]
(R/S)-OBN-4CN-BN	500	27	96	1.0	508	33	24.5	0.5	[10]
(*P,P*",P"')-/(M,M",M"')-BN5	497	44	87	1.3	506	48	22.0	1.9	[12]
(*P,P*",P"')-/(M,M",M"')-BN4	500	43	88	1.1	510	49	20.6	3.7	[12]
(P/M)-helicene-BN	520	46	98	2.0	524	50	30.7	2.2	[13]
(P/M)-BN-Py	527	35	90	0.52	532	38	31.0	0.435	[14]
M,M-RBNN	617	38	96	1.40	617	48	36.6	1.91	[15]
R-DOBP	536	-	1	0.25	716	-	1.9	-	[16]
R-HDOBP	534	-	2	0.15	700	-	0.7	-	[16]
Hel-BNN	572	95	60	2.12	567	62	21.9	0.468	This work

[a] Measured in solution.

Table S4. Cartesian coordinates of optimized S_0 state structure.

***P*-Hel-BBN**				***M*-Hel-BBN**			
Atom	X	Y	Z	C	X	Y	Z
C	4.2314	-0.5544	1.2849	C	4.72574	-0.09824	-0.8379
C	-0.0172	1.2797	-2.2358	C	-1.33474	2.26134	1.38398
C	-0.4162	2.3913	-2.8996	C	-2.24879	3.30673	1.75134
C	-1.7239	2.5944	-3.188	C	-3.66683	3.171	1.55553
C	-6.4743	-2.9989	-0.2458	C	-6.02664	-4.36039	-0.34371
C	-0.4064	-4.7108	1.4575	C	0.47359	-4.92666	-0.48315
C	-1.3912	-4.1771	0.7292	C	-0.77414	-4.33236	-0.51471
C	-1.2214	-2.9835	0.1271	C	-0.89813	-2.94979	-0.35676
N	-0.1051	-2.3484	0.2411	N	0.20492	-2.18803	-0.11715
C	0.8656	-2.8454	0.9104	C	1.4521	-2.754	-0.1764
C	0.7371	-4.0261	1.5464	C	1.59578	-4.12884	-0.34706
C	2.0214	-2.1506	1.0052	C	2.60229	-1.86336	-0.21147
C	-2.2361	-2.4358	-0.5892	C	-2.19199	-2.28819	-0.41123
C	3.2329	-2.6345	1.3509	C	3.93875	-2.26409	-0.11281
C	4.3509	-1.8838	1.468	C	5.00727	-1.39833	-0.39607
C	3.0259	-0.0478	1.0096	C	3.40601	0.33766	-0.94403
C	1.9545	-0.8226	0.8436	C	2.36695	-0.53793	-0.58188
C	-1.9752	-1.2551	-1.1578	C	-2.2927	-0.94821	-0.02355

C	-2.8711	-0.5401	-1.8356	C	-3.54964	-0.32123	0.09031
C	-4.1136	-0.9973	-2.0093	C	-4.7083	-1.0003	-0.28357
C	-4.4385	-2.1996	-1.4893	C	-4.63259	-2.31293	-0.75389
C	-3.4923	-2.8818	-0.8005	C	-3.37413	-2.93299	-0.7912
C	2.5685	1.2003	0.8784	C	2.7394	1.54576	-1.35191
C	1.2366	1.1474	0.6856	C	1.35983	1.31792	-1.22155
N	0.9254	-0.0998	0.646	N	1.13375	0.05351	-0.65482
C	3.2592	2.3406	0.9455	C	3.23103	2.77781	-1.83192
C	2.6134	3.5095	0.8102	C	2.37	3.77014	-2.22394
C	1.27	3.4941	0.6477	C	0.95642	3.50644	-2.23037
C	0.5781	2.3261	0.6026	C	0.43392	2.25328	-1.76893
N	-0.8616	-0.6547	-1.0755	N	-1.28267	-0.11907	0.38236
C	-0.9414	0.4179	-1.7706	C	-1.89223	1.06274	0.83585
C	-2.2077	0.5619	-2.1987	C	-3.2794	0.96749	0.65063
C	-2.6153	1.6343	-2.8813	C	-4.15223	2.01618	1.00577
B	-0.3458	-0.8509	0.3382	B	0.16806	-0.60694	0.38613
C	5.6903	-2.5441	1.8275	C	6.44209	-1.91333	-0.23033
C	6.0535	-3.5964	0.7556	C	6.66746	-3.12783	-1.14574
C	6.876	-1.5544	1.9077	C	7.4838	-0.8504	-0.58997
C	5.5711	-3.2256	3.2089	C	6.66919	-2.32792	1.23259
C	3.4328	4.7849	0.8653	C	2.90292	5.0925	-2.69707
C	-2.2201	3.8216	-3.9268	C	-4.60573	4.27796	1.9423
C	-5.8474	-2.7935	-1.6434	C	-5.8662	-3.10005	-1.20927
C	-6.821	-1.9007	-2.4479	C	-7.15099	-2.27592	-1.08962
C	-5.7592	-4.1475	-2.3824	C	-5.69791	-3.51013	-2.68134
C	0.6036	4.661	0.5245	C	0.04333	4.45449	-2.74907
C	-0.7264	4.7125	0.372	C	-1.29796	4.1726	-2.87372
C	-1.4178	3.5692	0.3524	C	-1.78714	2.9088	-2.50329
C	-0.7577	2.4099	0.4717	C	-0.93631	1.97193	-1.96463
C	1.2985	1.0249	-2.1162	C	0.04576	2.48634	1.57256
C	2.2254	1.9031	-2.5223	C	0.52297	3.65803	2.11211
C	1.8325	3.0525	-3.0838	C	-0.36845	4.67277	2.49144
C	0.5254	3.2776	-3.2822	C	-1.72016	4.49418	2.3094
C	-1.294	-0.6174	1.6146	C	0.71107	-0.67349	1.92677
C	-0.7881	-0.86	2.8409	C	1.93934	-0.20003	2.40855
C	-1.5194	-0.7287	3.9583	C	2.29937	-0.32042	3.74833
C	-2.8019	-0.3493	3.8797	C	1.43754	-0.93224	4.65291
C	-3.3321	-0.1009	2.6746	C	0.21014	-1.41166	4.20488

C	-2.5849	-0.2326	1.5673	C	-0.14073	-1.27685	2.86531
H	5.0795	0.1325	1.4006	H	5.53406	0.57741	-1.09649
H	-5.9137	-3.7282	0.3789	H	-5.15854	-5.02237	-0.42104
H	-6.5147	-2.038	0.3164	H	-6.15175	-4.09612	0.71114
H	-7.5145	-3.3891	-0.3212	H	-6.90695	-4.93118	-0.66017
H	-0.5335	-5.6789	1.9698	H	0.57249	-6.00186	-0.5966
H	-2.3196	-4.7638	0.6734	H	-1.66458	-4.93257	-0.64235
H	1.5299	-4.4754	2.1637	H	2.59059	-4.5499	-0.41236
H	3.3488	-3.7154	1.5099	H	4.16147	-3.2794	0.20099
H	-4.8218	-0.3764	-2.5732	H	-5.66702	-0.49983	-0.19873
H	-3.798	-3.8452	-0.3735	H	-3.322	-3.95797	-1.14231
H	4.3486	2.3189	1.1018	H	4.3049	2.94177	-1.88414
H	-3.6712	1.7223	-3.1803	H	-5.22147	1.89765	0.84633
H	6.1124	-3.1302	-0.2544	H	6.51262	-2.85961	-2.19569
H	5.3191	-4.4293	0.6981	H	5.98691	-3.95102	-0.90717
H	7.0403	-4.067	0.9668	H	7.69114	-3.50327	-1.03608
H	7.0515	-1.0375	0.937	H	7.39985	-0.5343	-1.63508
H	6.728	-0.7888	2.7026	H	7.39695	0.03596	0.0471
H	7.8257	-2.0793	2.1583	H	8.48908	-1.26034	-0.44955
H	5.2856	-2.4872	3.9926	H	6.52197	-1.47769	1.9061
H	4.814	-4.04	3.2249	H	5.98114	-3.11993	1.54346
H	6.536	-3.6877	3.5177	H	7.69063	-2.70065	1.36971
H	3.1174	5.4264	1.7193	H	2.51143	5.9247	-2.10042
H	3.3442	5.354	-0.0882	H	2.63659	5.29225	-3.74178
H	4.5198	4.5951	1.0082	H	3.99309	5.11545	-2.62293
H	-1.9859	4.7471	-3.3528	H	-4.38756	5.20648	1.40181
H	-1.7697	3.8859	-4.9432	H	-5.63848	3.99876	1.71865
H	-3.3233	3.8206	-4.0717	H	-4.54828	4.50726	3.01287
H	-6.4662	-1.7314	-3.4898	H	-7.11272	-1.37203	-1.70652
H	-6.9841	-0.9146	-1.957	H	-7.34939	-1.97921	-0.05435
H	-7.8257	-2.3731	-2.5351	H	-8.00308	-2.87269	-1.43048
H	-5.2854	-4.0232	-3.3829	H	-5.58943	-2.62912	-3.32181
H	-5.17	-4.9081	-1.8249	H	-4.81593	-4.14059	-2.83085
H	-6.7688	-4.5895	-2.541	H	-6.5724	-4.07566	-3.02263
H	1.1164	5.6357	0.5427	H	0.41609	5.42021	-3.07448
H	-1.2477	5.6789	0.2707	H	-1.97331	4.91873	-3.28269
H	-2.5143	3.5832	0.2333	H	-2.83629	2.66617	-2.64241
H	-1.3791	1.5153	0.4433	H	-1.30838	0.98848	-1.70788

H	1.6539	0.0697	-1.6999	H	0.75065	1.72013	1.29113
H	3.2986	1.6797	-2.4025	H	1.59294	3.7922	2.2394
H	2.5842	3.7858	-3.4209	H	0.0058	5.59763	2.92115
H	0.2675	4.2157	-3.799	H	-2.40328	5.28658	2.59653
H	0.2572	-1.1836	2.964	H	2.6359	0.28425	1.72868
H	-1.0684	-0.9369	4.9432	H	3.25764	0.06648	4.08507
H	-3.4101	-0.2391	4.7926	H	1.71664	-1.02887	5.69863
H	-4.384	0.2227	2.5968	H	-0.47885	-1.88307	4.90088
H	-3.0819	0.0156	0.6202	H	-1.11309	-1.64549	2.54292

Table S5. Cartesian coordinates of optimized transition state structure.

	TS		
Atom	X	Y	Z
C	4.17837	-0.82454	0.17467
C	-1.74588	2.86387	-0.91356
C	-2.2717	3.78212	-0.07118
C	-2.90821	3.39159	1.05627
C	-4.53121	-4.29943	1.14664
C	0.0272	-4.0904	-3.08614
C	-1.10352	-3.5214	-2.64739
C	-1.04827	-2.31534	-2.0527
N	0.06457	-1.71421	-2.00691
C	1.1762	-2.29654	-2.16774
C	1.18875	-3.50202	-2.76876
C	2.20718	-1.69399	-1.51769
C	-2.01949	-1.72921	-1.30374
C	3.28635	-2.44219	-1.17857
C	4.27748	-2.05695	-0.34775
C	3.17686	-0.04121	-0.22748
C	2.20229	-0.41101	-1.07378
C	-1.97996	-0.44889	-0.85787
C	-2.85974	-0.07805	0.08722
C	-3.81301	-0.86757	0.58661
C	-3.97171	-2.09153	0.05734
C	-3.06241	-2.47435	-0.86403
C	2.99271	1.24667	0.04792
C	2.00728	1.60051	-0.78009
N	1.43437	0.59524	-1.34711
C	3.63363	2.09369	0.85681

C	3.34168	3.4045	0.79334
C	2.57138	3.81955	-0.23785
C	1.95169	2.92119	-1.03969
N	-1.24849	0.55269	-1.22387
C	-1.76593	1.55505	-0.60957
C	-2.65049	1.21447	0.33008
C	-3.19117	2.08232	1.19015
B	0.12848	0.4257	-0.59558
C	5.47341	-2.93731	0.03939
C	5.45627	-4.35098	-0.58411
C	6.77274	-2.24567	-0.43502
C	5.51279	-3.11343	1.57432
C	4.03154	4.35649	1.74885
C	-3.4692	4.36745	2.06939
C	-5.11094	-3.0306	0.4849
C	-6.09794	-2.39566	1.49346
C	-5.94041	-3.41865	-0.76128
C	2.461	5.13254	-0.52213
C	1.90048	5.55138	-1.66553
C	1.43878	4.6451	-2.5346
C	1.42523	3.34696	-2.19933
C	-1.36718	3.24337	-2.14468
C	-1.43756	4.53057	-2.52195
C	-1.79697	5.46111	-1.63031
C	-2.21067	5.08362	-0.41322
C	0.21454	-0.0392	0.92979
C	0.33536	0.87231	1.90992
C	0.4193	0.49135	3.19436
C	0.3751	-0.81052	3.51691
C	0.25349	-1.72973	2.54861
C	0.17988	-1.3409	1.26762
H	4.94532	-0.42588	0.85392
H	-3.89253	-4.89157	0.45482
H	-3.91395	-4.03583	2.03587
H	-5.34241	-4.98184	1.48866
H	0.01139	-5.08865	-3.55444
H	-2.03089	-4.10337	-2.75996
H	2.10634	-4.06949	-2.98222

H	3.3557	-3.48184	-1.51588
H	-4.49783	-0.46291	1.34286
H	-3.17097	-3.51527	-1.1941
H	4.39796	1.72405	1.55657
H	-3.85966	1.72963	1.98904
H	5.47646	-4.31532	-1.69685
H	4.56942	-4.9386	-0.25552
H	6.35106	-4.93783	-0.27629
H	6.75811	-2.0851	-1.53734
H	6.93427	-1.25454	0.04353
H	7.67106	-2.8586	-0.19642
H	5.66202	-2.15501	2.11836
H	4.56563	-3.5664	1.94634
H	6.35025	-3.77808	1.88493
H	3.28269	4.99436	2.27279
H	4.76558	5.00403	1.21845
H	4.5921	3.82525	2.54988
H	-2.65417	5.01448	2.46792
H	-4.27004	5.00649	1.63503
H	-3.91013	3.85478	2.95355
H	-6.58515	-1.48398	1.07858
H	-5.60247	-2.13463	2.45575
H	-6.92211	-3.09827	1.75231
H	-6.33994	-2.51149	-1.27023
H	-5.3532	-3.99223	-1.51148
H	-6.80886	-4.05986	-0.48877
H	2.90487	5.91392	0.11412
H	1.88842	6.62276	-1.92575
H	1.07805	4.9743	-3.5223
H	1.07043	2.61784	-2.94567
H	-1.09693	2.49223	-2.90343
H	-1.19765	4.8179	-3.55747
H	-1.82489	6.52434	-1.92399
H	-2.58514	5.88267	0.24849
H	0.36852	1.944	1.65686
H	0.52314	1.24991	3.98847
H	0.4415	-1.12499	4.57203
H	0.2165	-2.80304	2.8061

H	0.08479	-2.12246	0.50047

3. Reference

[1] J.-D. Chai and M. H.-Gordon, Phys. Chem. Chem. Phys., 2008, 10, 6615.

[2] L. Kronik, T. Stein, S. Refaely-Abramson, R. Baer, J. Chem. Theory Comput., 2012, 8, 1515.

[3] H. Sun, C. Zhong, J. L. Brédas, J. Chem. Theory. Comput., 2015, 11, 3851.

[4] Martin, R. L. Natural transition orbitals. J. Chem. Phys., 2003, 118, 4775.

[5] T. Lu, F. Chen, J. Comput. Chem. 2012, 33, 580.

[6] Masui, K., Nakanotani, H. & Adachi, C. Org. Electron. 2013, 14, 2721-2726.

[7] Z. Ye, H. Wu, Y. Xu, T. Hua, G. Chen, Z. Chen, X. Yin, M. Huang, K. Xu, X. Song, Z. Huang, X. Lv, J. Miao, X. Cao, C. Yang, Adv. Mater. 2024, 36, 2308314.

[8] Z. P. Yan, L. Yuan, Y. Zhang, M. X. Mao, X. J. Liao, H. X. Ni, Z. H. Wang, Z. An, Y. X. Zheng, J. L. Zuo, Adv. Mater. 2022, 34, e2204253.

[9] X. J. Liao, D. Pu, L. Yuan, J. Tong, S. Xing, Z. L. Tu, J. L. Zuo, W. H. Zheng, Y. X. Zheng, Angew. Chem. Int. Ed. 2023, 62, e202217045.

[10] Y. Xu, Q. Wang, X. Cai, C. Li, Y. Wang, Adv. Mater. 2021, 33, e2100652.

[11] Y. Yang, N. Li, J. Miao, X. Cao, A. Ying, K. Pan, X. Lv, F. Ni, Z. Huang, S. Gong, C. Yang, Angew. Chem. Int. Ed. 2022, 61, e202202227.

[12] X. Wu, J. W. Huang, B. K. Su, S. Wang, L. Yuan, W. Q. Zheng, H. Zhang, Y. X. Zheng, W. Zhu, P. T. Chou, Adv. Mater. 2022, 34, e2105080.

[13] W. Yang, N. Li, J. Miao, L. Zhan, S. Gong, Z. Huang, C. Yang, CCS Chem. 2022, 4, 3463.

[14] Q. Wang, L. Yuan, C. Qu, T. Huang, X. Song, Y. Xu, Y. X. Zheng, Y. Wang, Adv. Mater. 2023, e2305125.

[15] G. Meng, J. Zhou, X. S. Han, W. Zhao, Y. Zhang, M. Li, C. F. Chen, D. Zhang, L. Duan, Adv. Mater. 2024, 36, e2307420.

[16] L. Zhou, F. Ni, N. Li, K. Wang, G. Xie, C. Yang, Angew. Chem. Int. Ed. 2022, 61, e202203844.